Journal of Ceramic Processing Research. Vol. 14, No. 4, pp. 557~562 (2013)

J O U R N A L O F
Ceramic Processing Research

Controlled band energetics in Pb-Fe-Nb-O metal oxide composite system to fabricate efficient visible light photocatalyst

K Vijayasankar[a], Neha Y. Hebalkar[a], H.G.Kim[b]* and Pramod H. Borse[a,]*

[a]*International Advanced Research Centre for Powder Metallurgy and New Materials (ARC International), Balapur PO, Hyderabad, AP, 500 005, India*

[b]*Korea Basic Science Institute, Busan center Busan 609-735, Korea*

We report here an efficient Pb-Fe-Nb-O based composite oxide photocatalyst prepared by simple solid-state reaction method. The low band gap semiconductors of Pb_2FeNbO_6, $FeNbO_4$, and composite (Pb_2FeNbO_6) : ($FeNbO_4$) system were synthesized under various thermal conditions, and further systematically investigated for their physico-chemical properties. The composite of Pb-Fe-Nb-O oxide formed at 1100 °C was found to be doubly efficient photocatalyst than $TiO_{2-x}N_x$, for the decolorization of methylene blue under solar radiation. This photocatalytic activity can be attributed to the role of Fe-*d*, Nb-*d* and Pb-*f* states in the band gap of (Pb_2FeNbO_6) : ($FeNbO_4$) system. The smaller band gap of this material additionally contributes to the improved visible light photocatalytic activity over UV-active TiO_2.

Key words: Composite, Lead Iron Niobate, Photocatalyst, Visible light, Solar radiation.

Introduction

Ternary and quaternary metal oxide photocatalysts of $Sr_2Nb_2O_7$ [1], $La_2Ti_2O_7$ [2], $Ni_xIn_{1-x}TaO_4$ [3], $K_3Ta_3Si_2O_{13}$ [4], $Sm_2Ti_2O_5S_2$ [5] and various other material systems [6-8] have been known to display enhanced photocatalytic activity in contrast to the conventional photocatalysts *viz.* $TiO_{2-x}N_x$ [9], $TiO_{2-x}C_x$ [10], TaON [11] and $(Ga_{1-x}Zn_x)(N_{1-x}O_x)$ [12]. This is because such crystal lattice posses' large population of catalytically active sites [1, 5]. Lead containing layered perovskite had been shown to posse additional advantage of effective light absorption of visible light photons from the solar electromagnetic spectrum [6, 13-16]. Such efficient visible light active photocatalysts are thus highly desirable in solar light water-splitting application, for energy generation as well as in pollutant degradation. Thus we attempt here a systematic investigation of Pb-Fe-Nb-O composite metal oxide as visible light photocatalyst.

As per the earlier reports [6] Pb-containing layered structures effectively alter the band gap of several different ternary metal oxides. Reports have demonstrated that Pb-6s orbital contributes to the top of valence band in $PbBi_2Nb_2O_9$ thereby reducing it's band gap [13], whereas to the bottom of conduction band in $BaSnO_3$: Pb [17] to converts the UV light active $BaSnO_3$ to visible light absorbing system. Such orbital dependent band energetics is important not only in converting the visible light inactive material to visible light absorbing material but also in achieving an improved version of visible light active photocatalyst [16]. We chose here Pb_2FeNbO_6 (PFNO) and $FeNbO_4$ (FNO) system to achieve a new mixed phase composite photocatalyst. PFNO and FNO are well known low band gap dielectric materials; those are popular for their potential applications in ferroelectrics, sensors, photocatalysis, photoelectrochemical hydrogen production *etc.* Hence the two systems were selected for making a composite photocatalyst. To fabricate such composite, the equi-molar oxide mixture was subjected to various thermal conditions with an aim to study the band gap dependent interplay of the mixed phase photocatalyst. The photocatalytic activity of the composite is studied by the photooxidation of methylene blue (MB) molecule under photons emanated from solar simulator. We report here a new mixed phase of Pb-Fe-Nb-O composite visible light photocatalyst synthesized by simple solid-state reaction method. The physico-chemical properties were systematically investigated and described in this paper.

Experimental

Synthesis of $FeNbO_4$, Pb_2FeNbO_6, (Pb_2FeNbO_6) : ($FeNbO_4$) photocatalyst

The $FeNbO_4$ (FNO), Pb_2FeNbO_6 (PFNO) and PFNO : FNO composite photo catalysts were prepared by the conventional solid state reaction method [18, 19]. Thus, respective precursors *viz.* PbO (LOBA Chemie, India, 98%), Fe_2O_3 (CDH, India, 98.5%), Bi_2O_3 (SRL, India, 99%) and Nb_2O_5 (LOBA Chemie, India, 99.5%) were mixed in desired stoichiometric ratio and ground in presence of

*Corresponding author:
Tel : +82-51-974-6104;+91-40-2445-2426
Fax: +82-51-974-6116 ; +91-40-2444-2699
E-mail: hhgkim@kbsi.re.kr ; phborse@arci.res.in

isopropyl alcohol, and then calcined at required temperature. Briefly, (i) In case of FNO the pelletized mixture was calcined at 1150 °C for 4 hrs to obtain a pure phase monoclinic phase FNO. (ii) For PFNO, the FNO powder obtained in previous step was used. A stoichiometric number of moles of FNO and PbO were mixed and calcined at 800 °C for 3 hrs. Further this mixture was pelletized and calcined again at 1125 °C for 2 hrs. (iii) In case of PFNO : FNO composite system, a stoichiometric ratio of Pb : Fe : Nb : : 1 : 2 : 2 was used to obtain a mixture. The pelletized mixture was heated at 800 °C followed by sintering in the temperature range of 1000ºC-1215 °C for more than 24 hrs under static air atmosphere. The PFNO : FNO powder samples were termed as PFNO : FNO-1000, PFNO : FNO-1050, PFNO : FNO-1100, PFNO : FNO-1150 and PFNO : FNO-1200, depending on the calcination temperature. The samples were used for various physico-chemical investigations.

For comparison, $PbBi_2Nb_2O_9$ and $TiO_{2-x}N_x$ were synthesized as reference, and used under the identical conditions of MB photocatalytic de-colorization experiments. $PbBi_2Nb_2O_9$ (PBNO) was prepared by SSR method by using a stoichiometric mixture of PbO, Bi_2O_3, and Nb_2O_5. After preheating the mixture at 800 °C for 24 hrs, the mixture was further calcined at 1100ºC for 24 hrs [13]. The $TiO_{2-x}N_x$ photocatalyst particles were prepared by hydrolytic synthesis method [20]. In this, ammonium hydroxide (NH_3 28-30%) was added drop-wise to the $TiCl_3$ solution kept at ice bath (0 °C) temperature, and stirred for 5 hrs under N_2 atmosphere. The white colored precipitate obtained was washed in steps with de-ionized water, isopropyl alcohol and calcined at 350 °C for 2 hrs after drying.

Characterization

The photocatalyst crystal structure was characterized by X-ray diffractometer; Model Bruker AXS D8 advance (using Cu K_α radiation, $\lambda = 1.54058$ A°). The XRD profiles were collected by a high resolution linear position sensitive LynxEye detector attached to Bruker system. The X-ray diffraction spectra were compared with the standard data in the JCPDS (Joint Committee Powder Diffraction Standards) for identification of the phase. The necessary experimental broadening was also taken care. The quantitative phase analysis was done by software provided with X-ray diffractometer. The specific surface area of the photocatalysts was estimated by the dynamic Brunauer-Emmett-Teller (BET) method, in which N_2 gas was adsorbed at 77 K using model ASAP 2020 V 3.00 H (Micrometrics, UK) system. The diffuse reflectance spectrum (DRS) of the photocatalyst powder was recorded in the wavelength range of 300-800 nm by using Perkin Elmer Lamda 650. The optical properties of the photocatalyst were investigated from the experimental observations. The elemental characterization was carried out by using X-ray photoelectron spectrometer Model Omicron equipped with anode. Vacuum of the order of ~ 1×10^{-9} Torr was maintained during XPS measurements. The samples were left in preparation chamber before the measurements to remove residual contents of water if any in the hygroscopic samples.

Photodegradation study

The photocatalytic activities of the catalysts investigated were evaluated *via* methylene blue (MB) depolarization experiments. MB is used as a model pollutant (indicator), which enables one to easily monitor the change in the absorbance at 664 nm. The initial concentration of MB in aqueous solution was 10 ppm. The catalyst (100 mg) was suspended in a special vertical illumination type photocatalytic reactor containing 100 mL of contaminated aqueous solution. Several MB concentrations from 5 ppm to 70 ppm were tried; The MB concentration was optimized to 10 ppm for these photodegradation experiments. The pollutant-photocatalyst mixture was used for the degradation experiment under simulated solar radiation illumination from Oriel model 300 W solar simulator consisting of an air mass filter (A.M 1.5). The photocatalyst reactor system was water and air cooled to maintain the constant temperature. The mixture was stirred under dark, prior to the illumination for at least 60 min to establish a stable adsorption-desorption mechanism between photocatalyst and MB. At given time intervals, about 5 ml of analytical suspension was taken from the reaction suspension by syringe. The photocatalyst powders and the MB solution were separated by a centrifugal machine. The decomposition of MB dye was monitored by measuring the absorbance of the samples using UV-visible spectrophotometer (Perkin Elmer Lamda 650 spectrophotometer) at regular interval of times. The absorption peak of MB at 664 nm was monitored as the probe of MB degradation [20]. The concentrations of MB were calculated using the Beer-Lambert law $A = \varepsilon cl$, where A is the absorbance at $_{max}$of MB, ε is the molar absorptivity of MB (79.5l x 10^3 l/mol cm), and l is the sample cell length (1 cm). MB degradation was expressed as C/C_0 *vs* photon-irradiation time, where C_0 was the initial concentration. Further, the results were correlated with the photocatalytic degradation by estimating the de-colorization efficiency,

$$\eta = \frac{C_0 - C}{C_0} \quad (1)$$

Where, C_0 and C are respectively the MB concentration before and after photocatalytic reaction.

Results and Discussion

Structural characterization of PFNO : FNO composite photocatalyst

The x-ray diffraction (XRD) spectra of the photocatalysts *viz.* FNO, PFNO, PFNO:FNO are shown in Fig.1 indicating the formation of respective

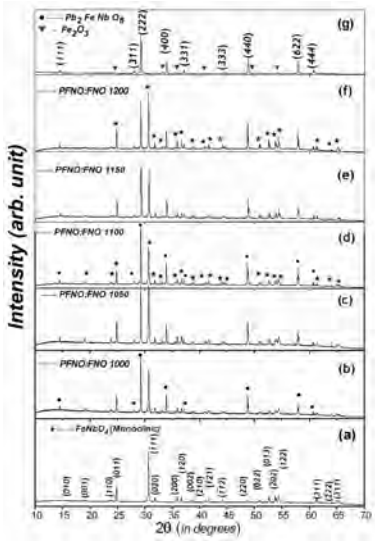

Fig. 1. X-ray diffraction spectra of (a) FNO calcined at 1150 ºC/ 4 hr, PFNO : FNO samples calcined at (b) 10000C, (c) 10500C, (d) 11000 ºC, (e) 11500 ºC, (f) 12000 ºC for 24 hs, and (g) Pb2FeNbO6 samples calcined at 1125 0C/2 hr. Impurity phase is indicated by solid triangle.

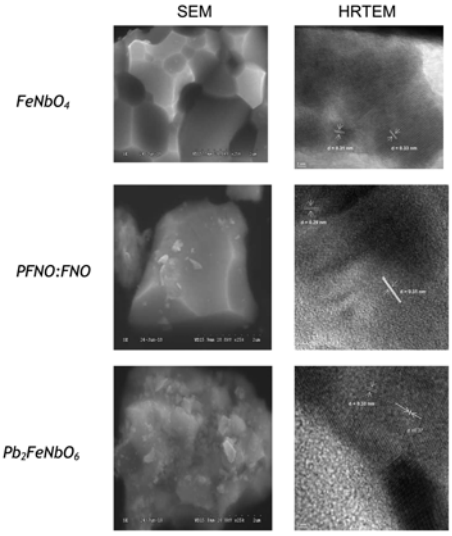

Figure SI. 1. SEM and HR-TEM studies of the FNO, PFNO and PFNO:FNO composite.

phases of monoclinic, cubic and composite system. Fig. 1(a) and (g) indicate the formation of monoclinic FNO and cubic PFNO phase respectively. Fig. 1(b-f) showing XRD spectra for the PFNO:FNO precursors calcined at various temperatures between 1000-1200 ºC, exhibited a mixture of respective PFNO and FNO. It is noteworthy to say that only Fig. 1(g) show some impurity peaks due to Fe_2O_3. The existence of FNO and PFNO is ascertained by the HR-TEM analysis of samples (see Fig.SI.1 in supplementary information*). The X-ray photoelectron spectroscopic (XPS) studies were used to ensure the oxidation states of the respective metal-ions in these samples (see Fig.SI.2 in supplementary information*). The results of the XRD quantitative phase analysis are presented in

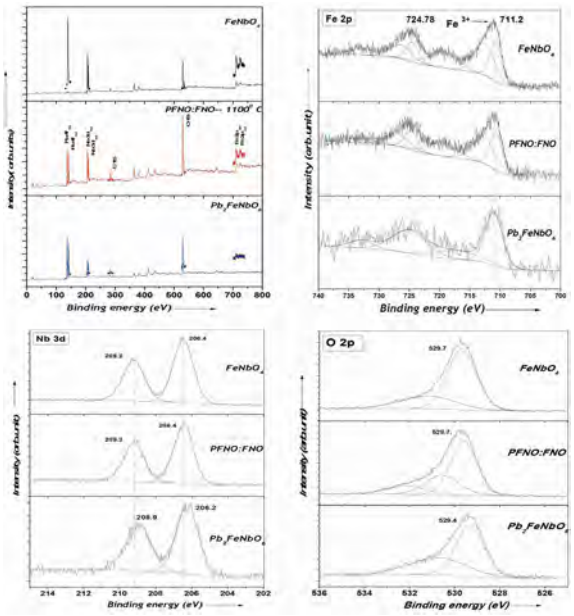

Fig SI. 2. XPS studies of FNO, PFNO and PFNO : FNO composite.

Table 1. Results of quantitative XRD phase analysis and bandgap values of PFNO:FNO samples obtained by calcination at various temperatures.

Calcination temperature for PFNO : FNO	Quantitative phases from XRD		Crystallite size	Bandgap energy
	PFNO	FNO		
1000 ºC	50.4	49.6	51 nm	2.14 eV
1050 ºC	49.4	50.4	51 nm	2.07 eV
1100 ºC	55.1	44.9	62 nm	2.06 eV
1150 ºC	44.0	56.0	60 nm	2.09 eV
1200 ºC	34.4	65.6	58 nm	2.10 eV

Table 1. The result shows that the PFNO : FNO calcined at temperature of 1100 ºC yields 62 nm sized particles and contains maximum fraction (~ 55%) of PFNO remaining being FNO. It is important to note that the variation in the PFNO and FNO can be expected due thermally induced diffusion dependent phase formation, as well as the partial probability of Pb-loss during calcination. The crystallite size was calculated from the full width at half maxima (FWHM) of respective main peak by using the Scherrer equation: $D = 0.89\,\lambda/(\beta \cos\theta)$, where D is the crystal size in nm, λ is the Cu $K_{\alpha 1}$ wavelength (1.5406 Å), β is the FWHM of the peak in radian, and θ is the corresponding diffraction angle.

Optical property of PFNO : FNO composite photo-catalyst

Fig. 2 shows the UV-Vis diffuse reflectance spectra of the PFNO : FNO samples calcined at various temperatures. In all the cases, the spectrum exhibit a sharp absorption edge around ~ 600 nm except for the sample calcined at ~ 1100 ºC, which shows absorption

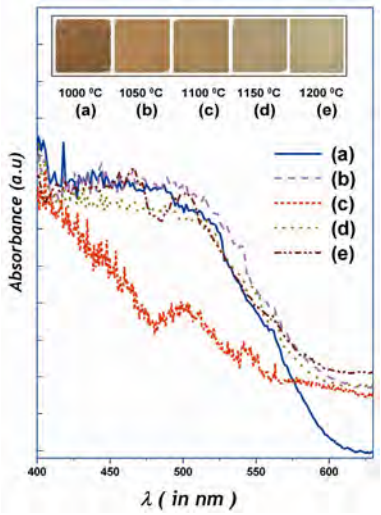

Fig. 2. Diffuse reflectance spectra of PFNO : FNO samples calcined at (a) 1000 °C (b) 1050 °C, (c) 1100 °C (d) 1150 °C (e) 1200 °C. The top inset shows the changes in the color with the calcination temperature.

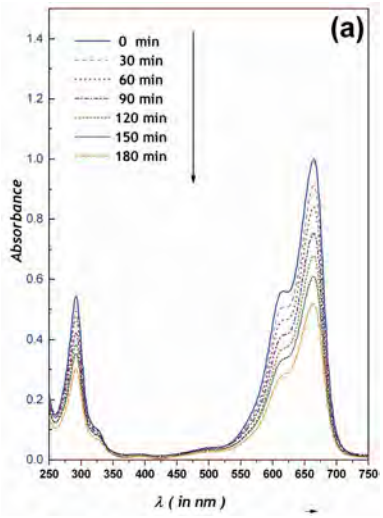

Fig. 3. (a) Optical absorption spectrum of MB absorption displaying the time dependent variation in its absorption intensity (~ 664 nm). The typical case of PFNO:FNO sample calcined at 1100 °C is shown here.

edge at still larger wavelength indicating the larger absorption capability of the photocatalyst. This observation is confirmed with the color of the samples. As shown in top-inset, the variation in the hue of respective sample clearly indicates the effect of calcination temperature. The band-gap estimated from the respective DRS spectra revealed the sample posses a band gap of around ~ 2.0 eV (See Table 1). The band gap lies in the range of 1.92 eV (PFNO) to 2.04 eV (FNO) which are the constituent counterparts for PFNO : FNO.

Methylene blue photo degradation study over PFNO : FNO composite photocatalysts

Time dependent spectrophotometric monitoring of irradiated MB/photocatalyst system is one of the best

Table 2. The percentage of MB photo degradation efficiency of various photocatalysts under solar radiation (1.5 AM) after 180 minutes of illumination.

Photocatalyst	Rate constant (κ)	Percentage MB discoloration efficiency %η
Methylene blue	4.68×10^{-4} min^{-1}	17.0
$TiO_{2-x}N_x$	6.84×10^{-4} min^{-1}	23.67
Pb_2 $FeNbO_6$ (PFNO)	8.16×10^{-4} min^{-1}	28.03
$FeNbO_4$ (FNO)	9.18×10^{-4} min^{-1}	31.97
$PbBi_2Nb_2O_9$	14.0×10^{-4} min^{-1}	43.40
PFNO:FNO-1000 °C	4.28×10^{-4} min^{-1}	24.78
PFNO:FNO-1050 °C	7.04×10^{-4} min^{-1}	25.19
PFNO:FNO-1100 °C	16.0×10^{-4} min^{-1}	48.18
PFNO:FNO-1150 °C	7.02×10^{-4} min^{-1}	23.34
PFNO:FNO-1200 °C	9.18×10^{-4} min^{-1}	25.62

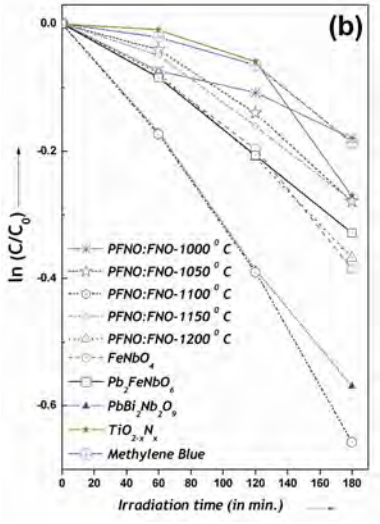

Fig. 3 (b) The logarithmic fractional change in the MB concentration (C/C_0) with the irradiation time for different photocatalysts *viz.* FNO, PFNO, PFNO : FNO samples calcined at 1000 °C, 1050 °C, 1100 °C, 1150 °C, 1200 °C, $PbBi_2Nb_2O_9$, and $TiO_{2-x}N_x$. The result of MB self degradation study is also shown. [MB concentration- 10 mg/L; Photocatalyst concentration-1g/L; solar simulator (1.5 AM)].

known ways to understand the photodegradation capability of a photocatalyst [20]. Fig. 3 shows the results of MB photodegradation study carried out over FNO, PFNO, PFNO : FNO, $PbBi_2Nb_2O_9$, and $TiO_{2-x}N_x$ photocatalyst systems. The PFNO : FNO (1100 °C) sample showed highest photodegradation activity which was found to be even better than $PbBi_2Nb_2O_9$, an efficient visible light photocatalyst.

Fig. 3(a) clearly confirms that as MB photodegradation reaction proceeds with an illumination time from 0 min to 180 min, the peak intensity due to MB electronic transition reduces to more than 50% after 180 min. This clearly indicates that PFNO : FNO (1100 °C)

photocatalytic decomposes. Further, to compare the photocatalytic activities of various photocatalysts, the rate constant (κ) and MB removal/discoloration efficiency were estimated and tabulated in Table 2. The kinetic curve MB photocatalytic degradation is obtained from the Fig. 3(a). It is shown in the Fig. 3(b) where logarithmic ratio of C/C_0 is plotted against the irradiation time. It plot clearly reveals that all the curves show a behaviour of linear variation with time, thereby indicating the photocatalytic degradation follows a first order reaction kinetics. The apparent reaction rate constants (κ) are shown in Table 2. The κ-value of PFNO : FNO-1100 was found to be maximum as also evident from the highest de-coloration. The $TiO_{2-x}N_x$ showed the expected value of κ-as 0.0006/min. The study clearly demonstrates that a high activity visible light photocatalyst has been achieved by using a very simple technique.

Efficient PFNO:FNO composite photocatalyst

Fig. 4 demonstrates that the composite photocatalyst is most efficient visible light photocatalyst among those discussed in the present study. Fig. 4(a) reveals that the photocatalytic activity was found to increase with the increase in the calcination temperature and displayed maximum efficiency for PFNO:FNO-1100. The samples calcined at other temperatures (other than 1100 °C) were 0.5 times less active. It can be noted from BET measurements that there is no significant variation in the value of specific surface area of PFNO:FNO-1100 sample as compared to others, thus ruling out the effect of surface area on the photocatalytic activity. Interestingly, the photocatalytic efficiency of PFNO:FNO-1100 composite photocatalyst was found to be higher than other known standard visible light photocatalyst ($PbBi_2Nb_2O_9$,$TiO_{2-x}N_x$). It is needless to say that composite outperforms its starting precursor counterparts (FNO and PFNO). This observation led to confirm that the interplay of PFNO:FNO band energetics is possibly playing a crucial role to render a favourable valence band edge in PFNO:FNO-1100 system for efficient MB oxidation. Such enhanced activity is expected in composite systems as due to efficient electron-hole charge separations. Incidentally, the calcination temperature dependent "crystal structure control" allows us to fine tune the band edges of PFNO:FNO and reach a favourable band energetics in PFNO : FNO-1100 to yield an efficient composite photocatalyst. The changes in the temperature dependent phase fraction have been evident from the XRD (Fig. 1) and optical studies (Fig. 2). The XRD studies indicate that for the samples PFNO : FNO-1000 and PFNO:FNO-1050, the individual PFNO and FNO phase co-exists in equal ratios, where as in PFNO:FNO-1150 and PFNO:FNO-1200, $FeNbO_4$ (monoclinic) phase constitutes the major phase fraction. The PFNO : FNO-1100 sample exhibit ~ 55% of cubic Pb_2FeNbO_6, which possibly favours the

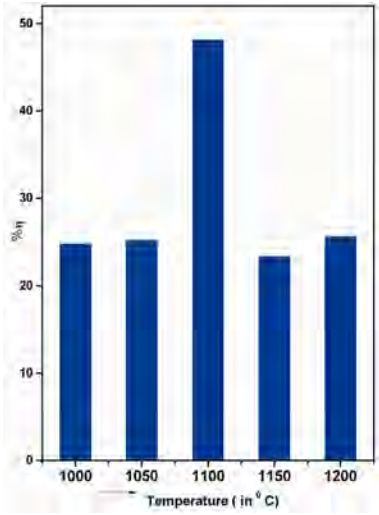

Fig. 4. (a) Bar graph showing the effect of PFNO:FNO calcination temperature on the MB photodegradation efficiency under simulated solar radiation.

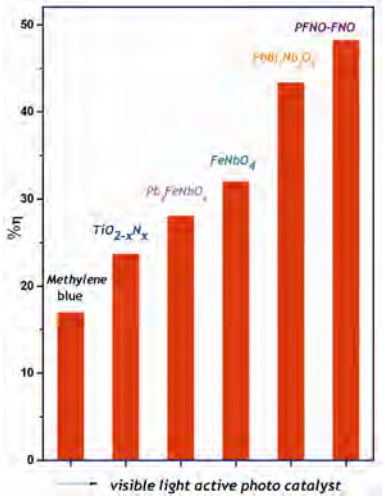

Fig. 4. (b) Graph shows the comparison of efficiency of PFNO:FNO-1100 with different known visible light active photocatalysts viz. FNO, PFNO, PbBi2Nb2O9, and TiO2-xNx. The result of MB self degradation is also included. [MB concentration-10 mg/L; Photocatalyst concentration-1g/L].

valence band by virtue of Fe-d, Nb-d and Pb-f states near the band gap. Thus it can be concluded that the existence of ~ 55% PFNO is necessary to achieve an efficient PFNO : FNO photocatalyst. In case of other samples it is probable that phase dependent changes in the density of states results in higher electron-hole recombination thereby making the photocatalyst less efficient.

Conclusions

The study of synthesis of Pb-Fe-Nb-O composite metal oxide visible light photocatalyst yielded an efficient MB degrading photocatalyst working under solar radiation. The composite photocatalyst made by calcination of stoichiometric mixture of Pb_2FeNbO_6 and $FeNbO_4$ at 1100 °C, yields highly efficient

photocatalyst. The composite photocatalyst exhibits larger Pb_2FeNbO_6 (55%) fraction than $FeNbO_4$. The study also shows that constituent precursors *i.e.* Pb_2FeNbO_6 and $FeNbO_4$ also show significant photocatalytic activity for MB degradation. The high MB photodecomposition efficiency of composite photocatalyst is attributed to its suitable band energetics. The composite photocatalyst is found to be twice efficient than $TiO_{2-x}N_x$.

Acknowledgment

The author KVS, acknowledges Department of Science and Technology (DST), India for the financial support given at ARCI, Hyderabad. The authors acknowledge Mr. K. Ramesh Reddy, L. Venkatesh, for their help in characterization, and R. Dom for useful discussions and help during the work.

References

1. H.G. Kim, D.W. Hwang, J. Kim, Y.G. Kim and J.S. Lee, Chem. Commun. 12 (1999) 1077-1078.
2. D.W. Hwang, H.G. Kim, J.S. Lee, J. Kim, W. Li, and S.H. Oh, J. Phys. Chem. B. 109 (2005) 2093-2102.
3. Z. Zou, J. Ye, K. Sayama, and H. Arakawa, Nature. 424 (2001) 625-627.
4. A.Kudo and H. Kato, Chem Lett. 20 (1997) 867-868.
5. A. Ishikawa, T. Takata, J.N. Kondo, M. Hara, H. Kobayashi, K. Domen, K., J. Am. Chem. Soc. 124 (2002) 13547.
6. H.G. Kim, O.S. Becker, J.S. Jang, S.M. Ji, P.H. Borse, J.S. Lee, J. Solid State Chem. 179 (2006) 1214-18.
7. R. Dom, R. Subasri, K. Radha and P.H. Borse, Solid State Commun. 151 (2011) 470-473.
8. H.G. Kim, P.H. Borse, J.S. Jang, and J.S. Lee, Adv. Mater. 23 (2011) 2088.
9. R. Asahi, T. Morikawa, T. Ohwaki, K. Aoki, Y. Tao, Science. 293 (2001) 269-72.
10. H,Y. Yun, H.Lee, J.B. Joo, N.D. Kim, J. Yi, Electrochem. Commun. 12 (2010) 769-772.
11. G. Hitoki, T. Takata, J. Kondo, M. Hara, H. Kobayashi, K. Domen, Chem. Commun. (2002) 1698-99.
12. D. Lu, T. Takata, N. Saito, Y. Inoue, K. Domen, Nature. 440 (2006) 295.
13. H.G. Kim, D.W.Hwang, and J.S. Lee, J. Am. Chem. Soc. 126 (2004) 8912-13.
14. H.G. Kim, P.H. Borse, W. Choi, J.S. Lee, Angew. Chem. Int. Ed. 44 (2005) 4585-4589.
15. K.G. Kanade, J.O. Baeg, K.J. Kong, B.B. Kale, S.M. Lee, S.J. Moon, C.W. Lee and S. Yoon, Intl. J. Hyd. Ene. 33 (2008) 6904-12.
16. Z. Shan, W. Wang, X. Lin, H. Ding, F. Huang, J. Solid State Chem. 181 (2008) 1361-66.
17. P.H. Borse, U.A. Joshi, H.G. Kim, S.M. Ji, J.S. Jang, and J.S. Lee, Appl. Phys .Lett. 90 (2007) 034103-05.
18. S.P. Singh, A.K. Singh, D. Pandeya, H. Sharma, and Om Parkash, J. Mater. Res. 18 (2003) 2677-87.
19. R. Sun, W. Tan, and B. Fang, Phys. Status Solidi A. 206 (2009) 326-331.
20. F. Ji, C. Li, and J. Zhang, Appl. Mater. Interf. 2 (2010) 1674-78.